The Third International Bridge Seismic Workshop, 3rd IBSW
Seattle, Washington, USA - October 1st to 4th, 2019

Comparative Assessment of Seismic Collapse Risk for Non-ductile and Ductile Bridges

Libo. Chen(1), Caigui. Huang(2), Leqia. He(3), Weidong. Zhuo(4)

(1) *Assistant Professor, College of Civil Engineering, Fuzhou University, lbchen@fzu.edu.cn*
(2) *Graduate Student, College of Civil Engineering, Fuzhou University, 1046571314@qq.com*
(3) *Assistant Professor, College of Civil Engineering, Fuzhou University, Leqia.He@fzu.edu.cn*
(4) *Professor, College of Civil Engineering, Fuzhou University, zhuowd@fzu.edu.cn*

Abstract

As a significant way to quantify the earthquake loss, risk assessment has been widely used in the field of seismic engineering. This study focuses on examining the seismic collapse safety and comparing the seismic behavior of reinforced concrete girder bridges with and without ductile detailing. On the basis, seismic collapse risk assessment for the two categories of bridges is conducted further. The numerical studies are performed based on the OpenSees platform. The finite element models of RC columns are established by introducing nonlinear shear springs in order to accommodate the different behaviors of flexure failure, flexure-shear failure, and shear failure. The adopted models are validated for the accuracy by using the data from the previous static cyclic-loading experiments. Case studies are conducted for three-span simply supported girder bridges, which are designed based on new and old seismic design criterion of China considering different ductile levels of the piers. By using incremental dynamic analysis, the collapse fragility curves are developed by considering the uncertainties of the ground-motion characteristics and those of the parameters of the structural materials. Based on the seismic hazard curve of a designated region, the seismic risk assessment of the bridges is carried out to quantify the associated improvements of the structural ductility of the bridges. The results regarding the seismic behaviors of the non-ductility and ductility of the bridges under seismic events can be used as the reference to implement specific policies for appraising and mitigating seismic collapse risk of the existing RC bridges.

Keywords: Non-Ductile Girder Bridge; Shear Failure; Collapse; Seismic Fragility; Seismic Risk Comparison

1. Introduction

Seismic risk assessment has been widely used in recent years to define the potential economic, social and environmental consequences of hazardous events which may occur in a specified period of time. As a popular way to evaluate the seismic safety of structures, seismic risk assessment can provide a reference for the decision-making regarding strengthening of bridge and risk mitigation after an earthquake. Previous studies have shown that the existing seismic performance estimates infuenced by uncertainty in the ductility during earthquakes [1]-[2]. The Non-ductile bridges, due to light or inadequately transverse reinforcement, have higher collapse probability and seismic risk than the ductile bridges. The main effects of transverse reinforcement on the seismic behavior are that different failure types of pier occurs between ductile and non-ductile girder bridges due to the difference of lateral support at bridge columns. The Non-ductile piers are usually subjected to shear failure or flexure-shear failure. In comparison, the ductile piers are usually subjected to flexure-shear failure or flexure failure. Shear failure is more dangerous with respect to the reduction in lateral shear strength, changes in post-failure deformation mechanism, losses of axial load-carrying capacity, and ultimately, bridge collapse. Therefore, it is critical that a finite element model is established to accurately predict the behaviors of the structures in the elastic range, inelastic range, and post-failure range, which can replace complex and expensive experiments.

An accurate numerical method is necessary to perform the nonlinear static pushover and time history analysis of non-ductile and ductile bridges. The fiber-based beam-column element is assigned to adequately describe the nonlinear flexural behavior of RC column [1]-[6]. This model could consider the spread of plasticity along the members and could be used under multidirectional loading conditions. However, it is insufficient to describe the shear flexibilities because the constitutive behavior of the material is unidirectional. To model the shear behavior of building columns, several proposals [4]-[6] have been made to predict the backbone of force-deformation relationship. Based on the shear spring element on the plastic hinge of the column, the post-failure behavior is predicted including stiffness degradation, strength

degradation, reduced strength during reloading, and pinching. Shear springs has been introduced to simulate the shearing effect of the bridge piers during the earthquake motion by Liu [7]. The accuracy of the different failure model is verified by comparing with the experimental results and the seismic performance of the pier is further studied.

Several studies have been conducted to assess the seismic risk of non-ductile structure in recent years. Shoraka [8] considered the effects of different collapse criteria of non-ductile frame structures on economic losses for seismic risk assessment. Padgett [9] evaluated and compared the cost effectiveness of different retrofitting strategies for non-ductile designed bridges based on seismic risk assessment. The comparative study about the seismic behavior of non-ductile and ductile structures has also been explored. Zakeri and Padgett [10] considered the limit state values of four different damage levels of component and system for non-ductile and ductile bridges. A comparative study of seismic fragility model shows that skew bridges without ductile detailing wil have higher probability of damage under the same ground motion as compared to those with ductile detailing. Ramanathan et. al [11] studied the seismic behavior of the ductile and non-ductile bridges. The fragility models were established for bridges that had different design criterions at piers and bearings. The results show significant improvement in seismic behavior when seismic design and details are considered in the analysis framework of bridges. As a great significant way to quantify the seismic performance of pre-and post-seismic designed bridges, seismic risk assessment has developed into a popular practice in engineering field. However, there are still limited comprehensively study, as the seismic risk assessment due to different failure types of piers, how to establish collapse fragility model of bridges, regarding exam the seismic collapse safety and for reinforced concrete girder bridges with and without ductile detailing.

By considering three kinds (flexure, flexure-shear and shear) of failure types of piers, this study establishes the finite element model of RC column by OpenSees platform [12]. The comparison with 6 column test data demonstrats that the proposed model can accurately predict the behavior of occurring failure and post-failure. The ductile and non-ductile bridge samples are designed by using Latin hypercube sampling method and the seismic collapse vulnerability model of bridge is obtained by using the incremental dynamic analysis method. According to the seismic hazard curve in a specific area, a comprehensive study of ductile and non-ductile bridges is established based on seismic risk curve to determine whether the existing RC bridges have sufficient seismic capacity.

2. The framework of seismic risk assessment

The seismic risk assessment framework is presented to formulate guidelines for bridge maintenance and seismic hazard prevention. The procedure combined the results of probabilistic seismic hazard models and fragility model for as-built bridges. The detailed analysis steps of seismic risk assessment are as follow:

2.1 Step 1: seismic hazard model

Seismic hazard is the probability that an earthquake will occur in a given geographic area, within a given window of time. In order to assess the risk of earthquake-induced collapse, structural analysis results are integrated with Probabilistic Seismic Hazard Analysis (PSHA). The probabilistic seismic hazard analysis can be used to determine the probability $H(a)$ that a particular ground motion intensity measure (A) exceeds a given threshold (a). In this context, the peak ground acceleration (PGA) was selected as the intensity measure of ground motion, which is equal to the amplitude of the largest absolute acceleration recorded. The probability $H(a)$ is expressed as follows:

$$H(a) = P\left[A \geq a\right] \tag{1}$$

The mean annual exceeding probability that an earthquake will occur in a given geographic area, with ground motion intensity, and under the given period and damping conditions can be expressed $\nu(IM)$. If

$\nu(IM)$ is approximated a linear function with the ground motion intensity measure in logarithmic space [13], Then Equation (1) becomes

$$H(a) = P\left[PGA \geq a\right] = v(IM) = k_0 (IM)^{-k} \tag{2}$$

Where k_0 and k are the shape coefficients of the seismic hazard curve associated with the site types. The coefficient k_0 scales the overall rate of ground motions and thus the probability of collapse, and k represents the steepness of the hazard curve. They are defined by the following formula respectively:

$$k = \frac{\ln(\nu_{DBE} / \nu_{MCE})}{\ln(IM_{DBE} / IM_{MCE})} \tag{3}$$

$$\ln(k_0) = \frac{\ln(IM_{DBE}) \cdot \ln(\nu_{MCE}) - \ln(IM_{MCE}) \cdot \ln(\nu_{DBE})}{\ln(IM_{DBE} / IM_{MCE})} \tag{4}$$

$$\left|\frac{dH(a)}{d(IM)}\right| = k_0 k (IM)^{-(k+1)} \tag{5}$$

Where IM_{DBE} and IM_{MCE} are the ground motion intensity magnitude of Design Basis Earthquake and Maximum Considered Earthquake. ν_{DBE}, ν_{MCE} are the mean annual exceedance probability of corresponding IM.

2.2 Step 2: seismic fragility model of bridge structure

The seismic fragility analysis is to find the probability of a structure reaching or exceeding a certain state of damage under a given earthquake motion[8]-[11]. The exceedance probability of the components or bridge systems are assumed to follow a lognormal distribution function, which can be expressed in the following expression:

$$P_i\left[D \geq C | IM\right] = \Phi\left[\frac{\ln(IM) - \ln(m)}{\beta}\right] \tag{6}$$

P_i represents the exceedance probability of the component, D and C are the seismic demand and the capacity of component. IM is the ground motion intensity measure, and here is represented by the PGA value. The exceedance probability of the components is described by a two-parameter lognormal distribution with median value, m and the dispersion ratio, β .

A bridge system is usually assumed as a serial system, which means that the damage of each component will cause the same degree of damage to the whole system. When referring to the damage state of a bridge system, the damage state is defined by the most severe damage state of each individual component. The exceedance probability of the bridge system under a given ground motion intensity measure can be approximated by using the maximum likelihood estimation method [14]. It's based on the number of damage samples and the total samples, by assuming the probability is follows the logarithmic normal distribution.

2.3 Step 3: seismic risk assessment of bridge structures

Herein, the seismic risk assessment process of bridge is conducted as follows: first, the probabilistic hazard curve is calculated based on Equation (2), to obtain the results of hazard curve as shown in Fig.8. Secondly the collapse probability is calculated by using the maximum likelihood estimation method, the seismic fragility curves are assumed obeyed the logarithmic normal distribution and fitted by Equation (6). Finally, the collapse deaggregation is estimated by combing the probability of collapse conditioned on the

intensity of the ground motion with seismic hazard curve describing the frequently each intensity threshold is exceeded [15]-[16]. The curves of seismic fragility and collapse risk are shown at Fig.1 (b) and Fig.1 (c) respectively. The mean annual collapse probability of the bridge is obtained by calculating the convolution of the seismic collapse deaggregation plot with the following formula:

$$\begin{aligned} v_c &= \int P(IM) \cdot \left| \frac{dH(a)}{d(IM)} \right| d(IM) \\ &= \sum_0^\infty P(IM) \cdot \left| \frac{dH(a)}{d(IM)} \right| \Delta(IM) \end{aligned} \tag{7}$$

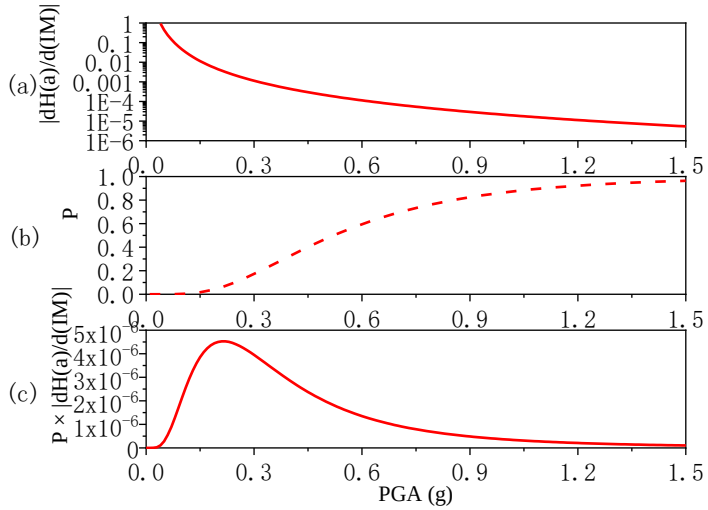

Fig.1 – The process of seismic risk assessment

3. Proposition and verification of numerical models for bridge columns

3.1 Prediction of failure modes

Due to the various material and geometric parameters of the piers, different failure types (flexure failure, flexure-shear failure and shear failure) may happen during earthquakes. In order to accurately simulate the seismic response of piers, each failure mode of piers requires a unique analytical model. Therefore, it is necessary to predict the failure mode of structures before the modeling process. In this context, the ASCE/SEI 41Concrete provision [17] is selected to predict the failure mode of the RC bridge pier, and V_p / V_n is used as the criterion for determining the structural failure mode, as shown in Table 1. Herein, V_n is the shear strength of structures, which is calculated by Equation (8) in reference to the United States ASCE 41-06 [17]. V_p is the shear demand of the plastic hinge area of the reinforced concrete pier, $V_p = M_{max} / h$, and $M_{\max}$ is the maximum bending moment of the section of the pier. It can be obtained by XTRACT software analysis, and h indicates the pier height [7]. In order to simplified calculating model, it's assumed that the transverse reinforcement conforming details to 135° hooks, and k value is 1.

$$\begin{cases} V_n = V_c + V_s \\ V_c = \left(\dfrac{\sqrt{f_c'}}{2M/Vd} \sqrt{1 + \dfrac{2P}{\sqrt{f_c'} A_g}} \right) 0.8 A_g \\ V_s = \dfrac{A_s f_{yt} d}{s} \end{cases} \tag{8}$$

Where V_c and V_s respectively represent the shear strength contributed by concrete and transverse reinforcement, Ag is the cross-sectional area of the pier, $f_c^{'}$ is the concrete strength, M/Vd is the shear span ratio, P is the axial load, A_v is the cross-sectional area of transverse reinforcement, f_{yt} is the transverse reinforcement yield strength, and s is the transverse reinforcement spacing.

Table 1 – classification of columns for determination of modeling parameters

Transverse Reinforcement Details	**ACI conforming details with 135° hooks**	**Closed hoops with 90° hooks**	**Other (including lap spliced transverse reinforcement**
$V_p / (V_0 / k) \le 0.6$	flexure failure	flexure-shear failure	flexure-shear failure
$0.6 < V_p / (V_0 / k) \le 1$	flexure-shear failure	flexure-shear failure	shear failure
$V_p / (V_0 / k) > 1$	shear failure	shear failure	shear failure

3.2 The finite element model of bridge

Based on Equation (8) and Table 2, the corresponding finite element model of the pier is established by using OpenSees software. The finite element model is relatively complex models with nonlinear fiber element and spring elements. The nonlinear fiber beam-column element is used to represent the pier columns, and the concrete and steel adopt the Concrete02 material and the Hysteretic material, see Fig.2. The springs in series at the ends of the columns are used to simulate the bond slip effect [18] and the shear strength and stiffness degradation [2].

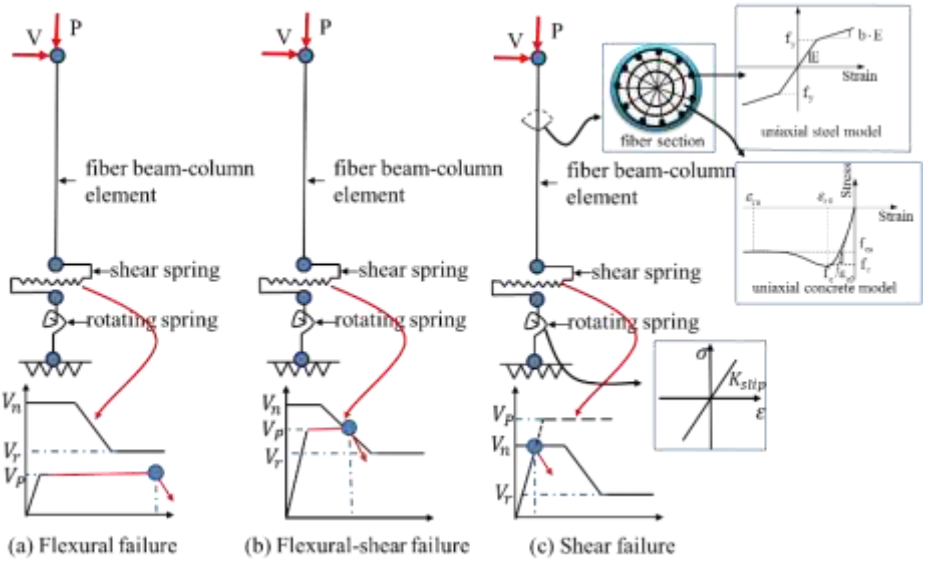

Fig.2 – The finite element model corresponding to various failure modes

In this paper, with respect to the different failure modes of bridge piers, the drift equations (9)-(11) when failure began to occur are adopted as proposed by Berry [19], Elwood [2] and Zhu [20]. They are used as the limit state surfaces to detect the flexure, flexure-shear and shear failure of the bridge piers. The shear limit curve, which was developed by Elwood [2], had to be shifted to the failure point proposed by Berry [19] and Zhu [20], as shown in Fig.2, using the delta function. When the structure fails, the backbone curve proposed by Elwood is used to calculate the degrading slope K_{deg} .

$$\frac{\Delta}{L}=3.25(1+k_e\frac{\rho_s f_{yt}}{f_c^{'}}\frac{d_b}{d})(1-\frac{P}{A_g f_c^{'}})(1+\frac{L}{10d}) \tag{9}$$

$$\frac{\Delta}{L}=0.03+4\rho_s-0.025\frac{v}{\sqrt{f_c^{'}}}-0.025\frac{P}{A_g f_c^{'}}\geq 0.01 \tag{10}$$

$$\frac{\Delta}{L}=2.02\rho_s-0.025\frac{s}{d}+0.013\frac{a}{d}-0.031\frac{P}{A_g f_c^{'}} \tag{11}$$

Where Δ / L is the drift ratio of pier, k_e is the transverse reinforcement coefficient, ρ_s is the transverse reinforcement ratio, f_{yt} is the yield stress of the transverse reinforcement, $P / A_g f_c^{'}$ is the structural axial load ratio, and v is the nominal shear stress, s is the transversal-reinforcement spacing, a/d is the shear- span ratio.

3.3 Verification of different failure models

Partial test data, which had been downloaded from the Structural Performance Database of Pacific Earthquake Engineering Research Center Database (https://nisee.berkeley.edu/spd/search.html), is used for verification of the aforementioned failure modes. It includes the specimens with three various failure modes. The structural parameters of the piers used for the verification are provided in Table 2. The OpenSees software is used to establish the finite element model of different failure modes of piers. Comparisons of the hysteretic-loop between the finite element models and experimental results are shown in Fig.3. Figure (a) is with respect to of the shear failure model, Figure (b) is with respect to the flexure-shear failure model and

Figure (c) is with respect to the flexure failure model. The numerical results match the experimental data with a satisfactory accuracy. By comparing the simulated results with the experimental results, it is shown that the finite element model can accurately simulat the initial stiffness, shear failure point, strength degradation slope and residual shear strength of the structure.

Table 2 – Test data of piers

Serial number	1	2	3	4	5	6	7	8	9	10	11	12
Section width (mm)	152	200	400	275	200	400	457	457	400	500	305	500
Section depth (mm)	305	200	500	275	300	400	457	457	400	500	305	500
Pier length(mm)	876	300	825	450	300	1000	1473	1473	1600	2730	1372	1750
Span-to-depth ratio	2.87	1.5	1.65	1.64	1.5	2.5	3.22	3.22	4	5.46	4.5	3.5
Axial Load Ratio (%)	7.1	17	7.2	16.6	35	10	15.1	7.3	19.7	0.3	9.4	5.3
Concrete strength(MPa **)**	33.6	21.6	27.1	41.3	21	34.3	21.1	33.1	26	40	29	34.8
Longitudinal reinforcement strength (MPa **)**	496	371	318	363	371	436	434	331	308	305	448	371
Transverse reinforcement strength(MPa **)**	345	344	336	381	344	326	476	400	308	389	434	312
Longitudinal reinforcement ratio(%)	2.45	1.27	2.66	3.85	1.27	3.2	2.47	1.94	2.43	2.57	2.04	2.57
Transverse reinforcement ratio(%)	0.3	0.8	0.4	0.63	1.4	0.51	0.2	0.01	0.76	1.26	0.94	0.44
Test Configuration	DE	DC	DC	DC	DC	C	DC	DC	DE	C	C	C
Failure model	S	S	S	S	FS	FS	FS	FS	F	F	F	F

Note：1-Wight 1973, Spec.WS25033E [21] ; 2-Nagasaka 1982, HPRC10-63 [22]; 3-Imai 1986, No. 1 [23]; 4-Arakawa 1988, No. 28 [24]; 5- Nagasaka1982, HPRC 19-32 [22]; 6- Ang 1985, Spec. 17 [25]; 7-Lynn 1998, 2CLH18 [26]; 8-Sezen 2000 No. 1 [27]; 9-Davey 1975, Spec. 2 [28]; 10- Munro 1976, Spec. 1 [29]; 11- Ang 1981, No. 1 [30]; 12- Kunnath 1997, A2 [31]; S—Shear failure, FS—Flexure shear failure, F—Flexure failure ; DC—Double Cantilever, DE—Double Ended, C—Cantilever

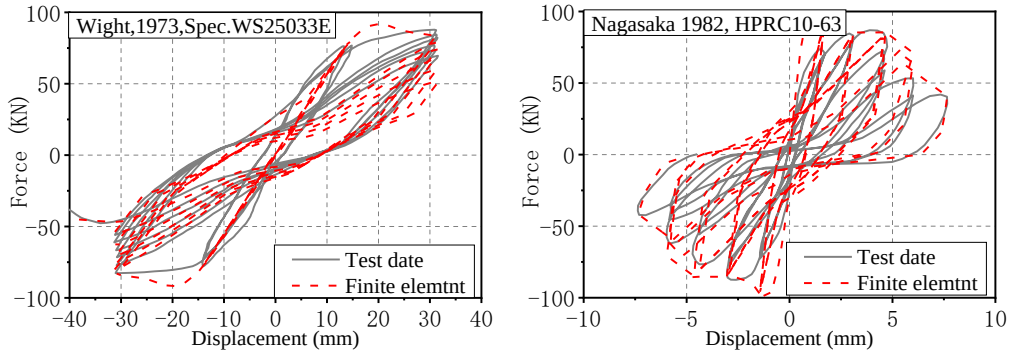

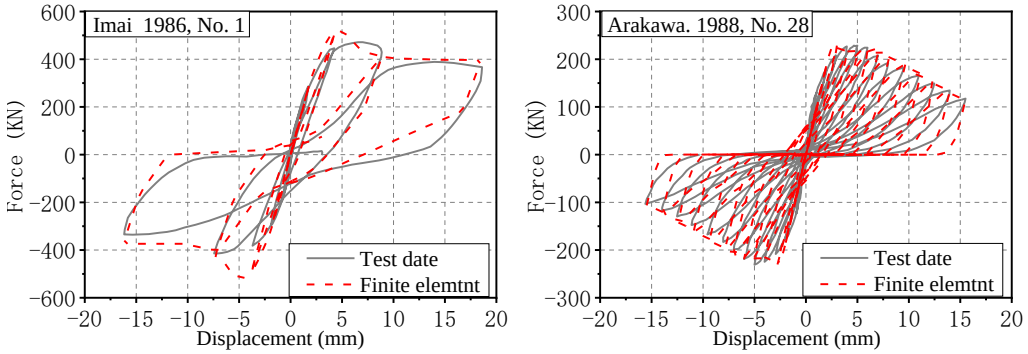

(a) Shear failure

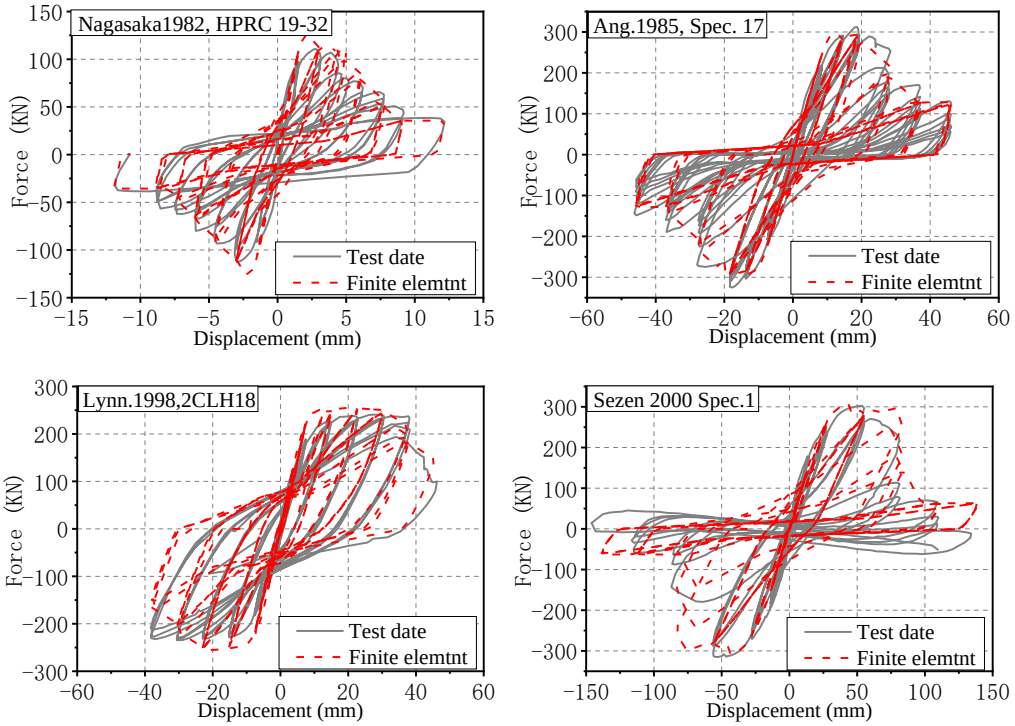

(b) Flexure–shear failure

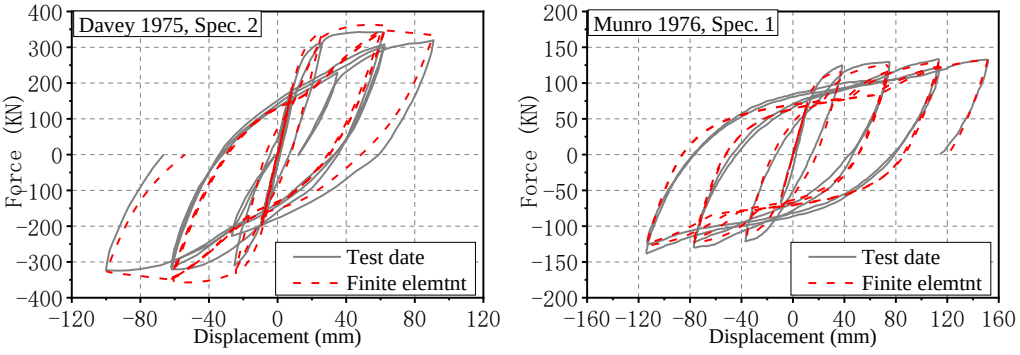

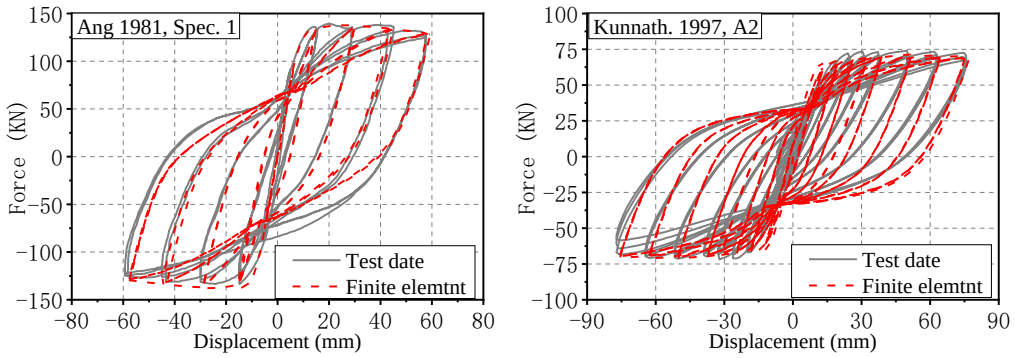

(c) Flexure failure

Fig.3 – Hysteretic loops of different failure modes for piers

4. Design details and simulation of bridge

4.1 Numerical models of three-span simply supported T-beam bridge

In this paper, a typical three-span simply supported T-beam bridge is selected as the research object, and the nonlinear dynamic response of the bridge is calculated using three-dimensional (3D) finite-element (FE) models in the OpenSees platform. Past analytical and experimental research has shown that the deck remains elastic during seismic excitations. Therefore, linear-elastic beam-column element is assigned to the deck. Considering the elastic perfectly plastic behavior of the plate rubber bearing under strong earthquakes excitations, the flat slider bearing element with bilinear constitutive law is used to model the bearings. The stiffness of the flat slider bearing element is calculated according to JT/T4-2004 Road Bridge Plate Rubber Bearing [32]. The model of the piers has been described in Section 2.2. In order to improve computational efficiency, the linear spring element at the end of pier is developed to simulate the pile-soil effect of the bridge [33]. A simplified abutment model is established based on the California Bridge Guidelines [34]. For more details, two rigid elements of superstructure width with a series zero-length element are developed to computer the longitudinal, transverse and vertical nonlinear response. In the longitudinal direction, a zero-length gap element connected rigid joint of various rigid element is assigned to simulate the collision effect between the girder and abutment. The passive soil pressures and pile-soil effect are considered using a zero-length spring element. In the transverse direction, a zero-length element at the end of the rigid link is selected to represent the backfill, wing wall, and pile system response. In the vertical direction, a bilinear spring element is defined at the rigid joint, with the stiffness of the flat slider bearing. The overall layout of the bridge is shown in Fig.4.

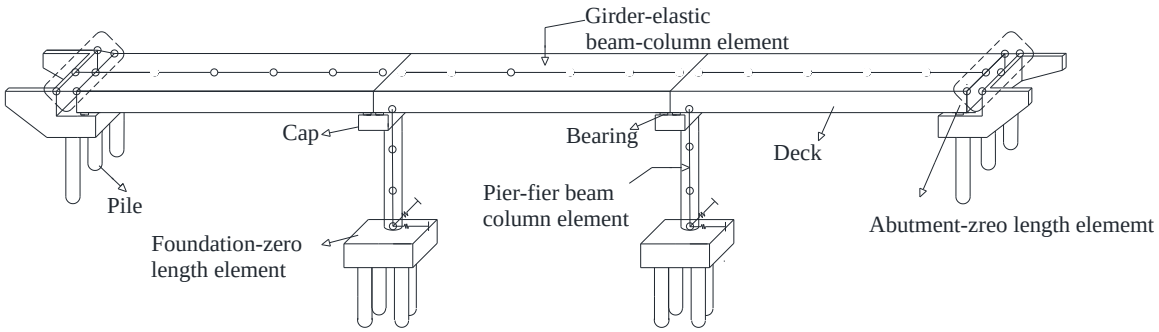

Fig.4 – Configuration details of the designed bridge

4.2 Selection of material parameters

A simply supported girder bridge is selected as the typical bridge model in this study. One of the primary differences of the ductile and non-ductile bridges have been captured on the uncertainties of material parameters. In contrast to older non-ductile RC bridges, modern code-conforming special moment bridges have higher value of these material parameters, which including concrete strengths, steel strengths, and the ratio of longitudinal reinforcement and transverse reinforcement. A Latin hypercube sampling (LHS) technique, commonly adopted for variance reduction, is used in this study to generate 60 ductile girder bridges, and 60 non-ductile girder bridge samples. According to the previous analytical and investigated research [35]-[39], all of the considered modeling parameters and their probability distributions are presented in Table 3. P1 and P2 are expressed the upper and lower bounds of the parameter if the parameter is obey the uniform distribution; for normal distribution and lognormal distribution, P1 and P2 are the mean and standard deviation of the parameters.

Table 3 – Random Variables and Distributions Incorporated in the Bridge Model

Parameter	Distribution type	Distribution parameter	
		P1	P2
Concrete strength (MPa)	Normal distribution	25(35)	4.5(4.5)
Shear elastic modulus of bearing(MPa)		1.18	0.16
Damping ratio		0.045	0.0125
expansion joint width (mm)		40	4
Longitudinal reinforcement ratio	uniform distribution	0.4%(1.0%)	1.0%(2.2%)
Transverse reinforcement ratio		0.1%(0.4%)	0.3%(1.2%)
Concrete density		0.9	1.1
Abutment initial stiffness (kN/mm/m)		11.5	28.5
Proportional coefficient of foundation horizontal resistance (kN/m^4)		60000	100000
Longitudinal reinforcement yield strength (MPa)	Lognormal distribution	5.7(5.8)	0.1(0.1)
Transverse reinforcement yield strength (MPa)		5.5(5.7)	0.1(0.1)

Note: The value in parentheses of Table 3 is the distribution of the ductile girder bridge.

4.3 Selection of ground motion

Seismic performance assessment and the potential probability for bridge system are affected by the selection of ground motions. The conditions of ground motion have been proposed by considering with various peak ground acceleration (PGA), peak ground velocity (PGV), fault interval, magnitude and combing the corresponding regulations for seismic response [40]. According to the above screening conditions, 60 near-fault records and 60 far-field records were selected from the Pacific Earthquake Engineering Research Center (PEER) Ground Motion Database and the European Ground Motion Database. The ground motion acceleration response spectrum is shown in Fig.5. In this paper, considering the randomness of bridge parameters, the non-ductile girder bridge and ductile girder bridge samples are designed by the Latin hypercube sampling method. The finite element model of bridge is established by OpenSees software, and the structural model is subjected to multiple ground motions with scaling to increasing amplitudes. Seismic response analysis of bridge matched with multiple near-far site records is executed, and the seismic fragility model of bridge is obtained by incremental dynamic analysis method.

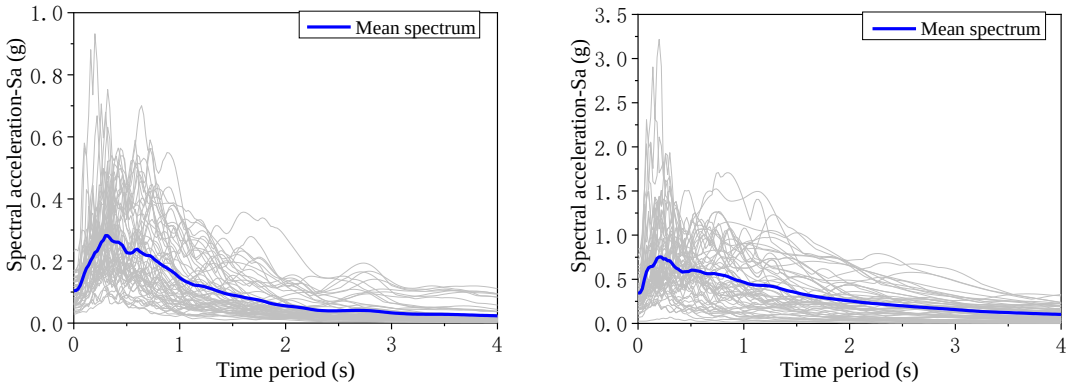

(a) Response spectra of far-field ground motions (b) Response spectra of near-fault ground motion

Fig.5 – Response spectrum of ground motions

5. Collapse fragility analyses of bridge system

5.1 Collapse performance assessment procedure

The collapse of the bridge is a serious damage type. In this paper, the sideway and vertical collapse of the piers or the relative displacement of girder exceeds support length are selected as the collapse criteria of the bridge. Zhu [20] assumed that the pier occurs vertical collapse when the shear strength drops to 0, which means that axial load exceeds the support capacity of pier. The drift ratio formula of axial failure is obtained according to the past experimental data. The regression formula for axial failure is shown in equation (12):

$$\Delta / L = 0.184\exp(-1.45\mu) \tag{12}$$

$$\mu = \frac{\dfrac{P}{A_{st} f_{yt} d_c / s} - 1}{\dfrac{P}{A_{st} f_{yt} d_c / s}\dfrac{1}{\tan\alpha} + \tan\alpha} \tag{13}$$

Where P is the axial load, A_{st} is the area of the transverse reinforcement, d_c is the distance from the center of the section to the center of the transverse reinforcement, s is the spacing of transverse reinforcement, and α is equal to 65° .

The Federal Emergency Management Agency (FEMA) defines the sideway collapse of the columns as follows: A slight increase in local ground motion intensity results in an infinitely large increase of structural displacement, which defined as the sideway collapse of the column [41]. The maximum drift ratio of the pier under each ground motion with increasing amplitudes is recorded, and the IDA curve is generated as shown in Fig. 6.

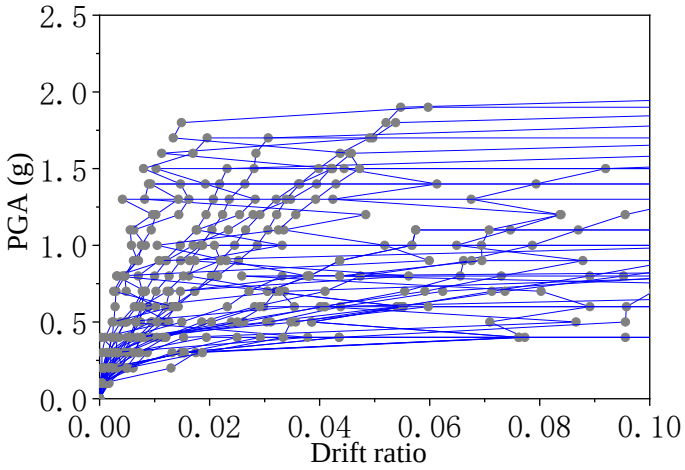

Fig.6 – IDA curves

The large relative displacement of the girder and the bearing under the action of an earthquake result in falling down of girder due to the deck is discontinuous. This collapse has been confirmed by previous earthquake investigation. Different design criterions have different calculating formulas for the fall prevention length of bridge [36]-[37]. The results are shown that the distance of the non-ductile girder bridge is the length between the edge of the bearing and the edge of the capping beam plus the width of the bearings, and the ductile beam bridge is 70+0.5Lcm. In this paper, the bridge length of span is 30m, and the anti-fall length of the non-ductile girder bridge and the ductile girder bridge are calculated to be 80cm and 85cm respectively.

In summary, the sideway and vertical collapse of the pier or the relative displacement of girder exceeds support length are defined as indexes of bridge collapse. The simply supported bridge is defined as a series system that the bridge will collapse if one of the indexes is achieved. The seismic response of the bridge is obtained by numerical analysis. The number of collapsed bridge under different ground motion intensity is counted. Assuming the collapse probability obeys lognormal distribution, the fragility curve is obtained by the method of maximum likelihood estimation [14].

5.2 Seismic fragility analysis of bridge system

Considering the uncertainties of design criterions and ground motion characteristics, the collapse fragility curve of the bridge system is established, as shown in Fig.7. The black line is expressed fragility curve of the non-ductile girder bridge, and the red line is represents the fragility curve of the ductile bridge. The solid line is the collapse curve of the bridge under the near-fault ground motion, and the broken line is the bridge collapse vulnerability curve under the far-field ground motion.

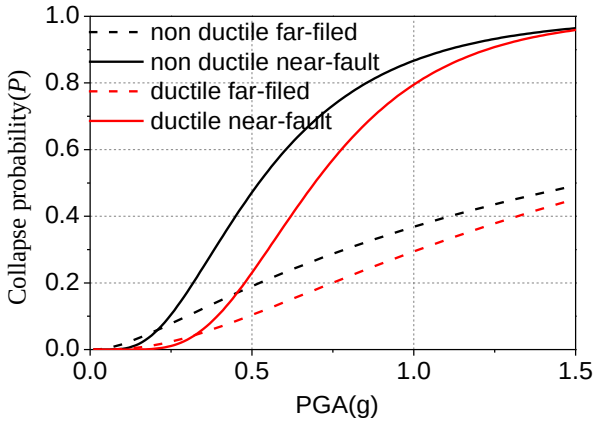

Fig.7 – Collapse fragility curve of the bridges

Table 4 – Fragility model parameters for non-ductile and ductile bridges

Parameter	Non-ductile Far field	Non-ductile near fault	Ductile far field	Ductile near fault
Median value m	1.54	0.52	1.68	0.69
Logarithmic standard deviation β	1.28	0.59	0.96	0.44

It can be seen from Fig.7 that the fragility curve of the same bridge, collapse probability under near-fault ground motion is greater than that under far-field. With respect to seismic performance of the bridges with or without ductile detailing, the collapse probability of non-ductile girder bridges are greater than that of ductile bridges under the same ground motions. The median and logarithmic standard deviation of the fragility curve is shown in Table 4. Compared with the median value of bridge whether consider seismic design and detailing to the ground motions, the results have been demonstrated that for the same collapse probability (50%) of the non-ductile bridge, the ground amplitude of far-field ground motion (0.14g) need to be improved for the bridges with ductile detailing, similarly need 0.17g under near-fault ground motions.

6. Seismic collapse risk assessment of bridge

6.1 Seismic hazard function

In this paper, a simply supported girder bridge located in China is selected as an example, and the design life of it is 100 years. The site type of the bridge is Class II, and the seismic fortification intensity is 7 degrees. By reviewing the specification [37], it can be seen that the recurrence periods of design earthquakes and rare earthquakes are 100 years and 1000 years respectively, and the annual excess probability ν_{DBE} and ν_{MCE} can be calculated to 0.01 and 0.001. The acceleration PGA with the 100-year surpass probability is calculated through the surpass probability 10 percent in 50 years [42]. Illustrative results show that the ground motion intensity magnitude of Design Basis Earthquake IM_{DBE} and Maximum Considered Earthquake IM_{MCE} is 0.049 g and 0.0132 g. Bring ν_{DBE}, ν_{MCE}, IM_{DBE}, and IM_{MCE} into equation (3) and (4), k and k_0 can be calculated and which is equal to 2.33 and 8.9×10^{-6} respectively. Bring k and k_0 into equation (2) and get:

$$H(a)=\nu(IM)=8.9\times10^{-6}(IM)^{-2.33} \tag{14}$$

$$\left|\frac{dH(a)}{d(IM)}\right|=8.9\times10^{-6}\times2.33(IM)^{-3.33} \tag{15}$$

According to formula (15), the seismic hazard curve of the site is obtained. IM is the peak ground acceleration PGA. Fig. 8 is shown the seismic hazard curve in logarithmic vertical coordinate. The horizontal coordinate indicates the ground motion intensity, and the ordinate indicates the occurrence probability of ground motion intensity exceeding a given threshold.

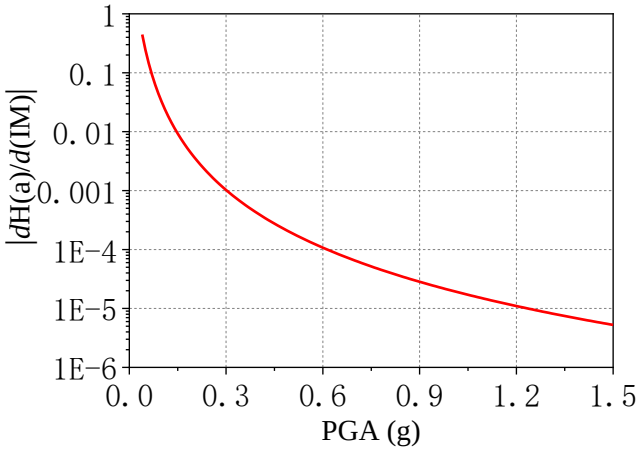

Fig.8 – Curve of the seismic hazard

6.2 Seismic risk assessment

In this paper, the seismic collapse deaggregation of the bridge is developed by integrating the product of the seismic hazard curve examined in detail in Section 5.1 and the collapse fragility curve of Section 4.2. The detailed process of bridge seismic risk assessment can be found in Section 1. The deaggregation of bridges with or without ductile detailing are shown in Fig 9. Fig.9 (a) shows the seismic collapse deaggregation of the ductile and non-ductile girder bridges during the far field ground motions, and Fig.9 (b) illustrates the collapse deaggregation under the near-fault ground motions. The black line is the seismic deaggregation of the non-ductile girder bridges, and the red line is the seismic deaggregation of the ductile girder bridges.

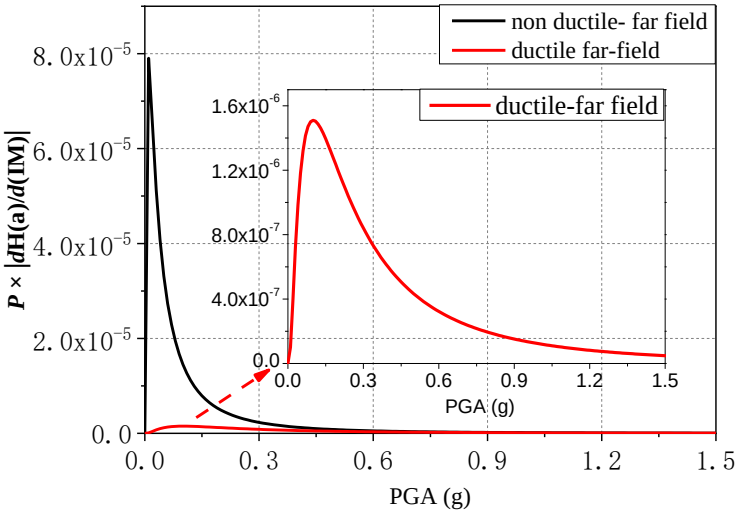

(a) Bridge collapse deaggregation plot under far-field ground motions

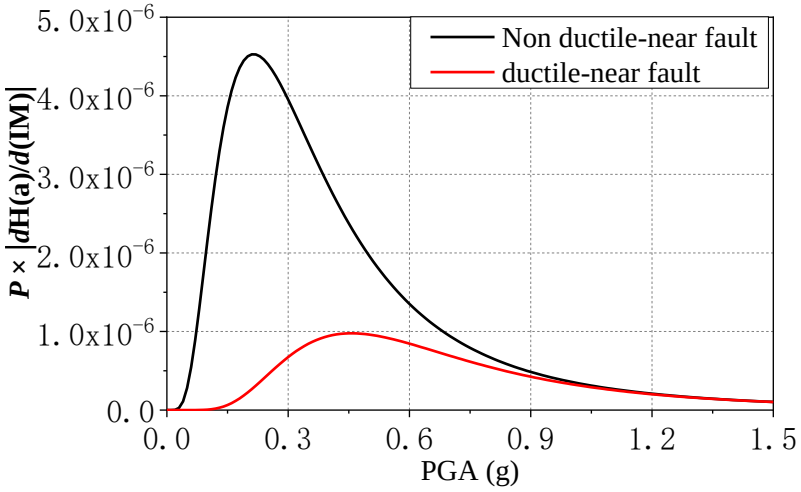

(b) Bridge collapse deaggregation plot under near-fault ground motions

Fig.9 – Seismic collapse deaggregation plot of the bridge

Assuming that the collapse probability obeys the lognormal distribution, the mean annual collapse probability v_c of the bridge can be calculated:

$$v_c = H(m)\exp(1/2k^2\beta^2) \tag{16}$$

Where m and β are represent the media and logarithmic standard deviations of the collapse fragility model, respectively. The mean annual collapse probability of bridges with and without considering seismic design under different ground motions are shown in Table 5.

Table 5 – Mean annual collapse probability of bridge

Mean annual collapse probability	**Non-ductile far field**	**Ductile far field**	**Non-ductile near fault**	**Ductile near fault**
v_C	2.78×10^{-4}	3.24×10^{-5}	1.05×10^{-4}	3.57×10^{-5}

The comparative results of deaggregation, as shown in Fig.9 (a), show that the bridge with and without seismic design have the highest risk probability when the PGA is 0.05g and 0.10g during the far-field ground motions. In comparison, the corresponding collapse probability of bridge is 0.37% and 0.17% to these ground motion intensities. Fig.9 (b) shows the collapse deaggregation of bridge with ductile and non-ductile design criterion to near-fault records, the highest risk probability (PGA equal 0.21g and 0.46g) corresponds with collapse probability of bridge is 6.0% and 17.7%. Illustrative results show that the structural collapse risk curve is not only related to the collapse probability of the structure under certain ground motion intensity, but also to the occurring probability of the ground motion intensity exceeding a given threshold.

The difference of seismic detailing may cause variation of the annual average collapse frequency v_c of the bridge to the same ground motion exaction. It can be seen from Table 5 that a mean annual frequency of collapse of non-ductile RC bridges is approximately 7.6 times higher than that of corresponding results for modern code-conforming special RC bridges under far-fault ground motions, and approximately 2.4 times under near -fault ground motions.

7. Conclusions

Taking a three-span simply supported girder bridge as the reference bridge type, the bridge sample is designed considering the uncertainties of material parameters. The finite element model of bridge with or without seismic design and detailing is established by OpenSees software. Each bridge is randomly matched with the near-far site ground motion records. The bridge collapse fragility model is developed based on the maximum likelihood estimation method, and the collapse risk is computed by integrating fragility model and seismic hazard curve. A comparison of seismic risk assessment for ductile and non-ductile bridges has been conducted, and the main conclusions are as follows:

The finite element model of pier column with different failure modes is established by the predicted results base on the criterion of failure mode. The finite element simulating results were compared with the experimental data of flexure failure, flexure-shear failure and shear failure. The comparative results show that the numerical model of the pier used in this paper can simulate the static response of its three failure modes.

According to the results of the collapse deaggregation, the ground motion with high intensity amplitude, which will cause high collapse probability of bridges, has little contribution to the mean annual collapse risk probability due to its small frequency. Therefore, the structural collapse deaggregation is not only related to the collapse probability of the structure under certain ground motion intensity, but also to the occurring probability of the ground motion intensity exceeding a given threshold.

The difference of seismic detailing may cause various result of the mean annual collapse frequency v_c of the bridge to the same ground motion exaction. Comparing the mean annual collapse probability of bridges, it can be seen that the mean annual collapse frequency of ductile girder bridges is smaller than that of non-ductile girder bridges. This can be a good proof of the new criterion for improving the seismic performance of bridges.

8. References

[1] MOEHLE J P, SEZEN H. Seismic tests of concrete columns with light transverse reinforcement. *ACI Structural Journal*, 2006, 103(6):842-849.

[2] ELWOOD K J, MOEHLE J P. Drift capacity of reinforced concrete columns with light transverse reinforcement. *Earthquake Spectra*, 2005, 21(1):71-89.

[3] FILIPPOU F C, NEUENHOFER A. Evaluation of nonlinear frame finite-element models. *Journal of Structural Engineering*, 1997, 123(7):958-966.

[4] ELWOOD K J. Modelling failures in existing reinforced concrete columns. *Canadian Journal of Civil Engineering*, 2004, 31(5):846-859.

[5] IBARRA L F, MEDINA R A, KRAWINKLER H. Hysteretic models that incorporate strength and stiffness deterioration. *Earthquake Engineering and Structural Dynamics*, 2005, 34(12):1489-1511.

[6] LEBORGNE M R, GHANNOUM W M. Analytical element for simulating lateral-strength degradation in reinforced concrete columns and other frame members. *Journal of Structural Engineering*, 2014, 140(7): 165-180.

[7] LIU KY, WITARTO W, CHANG K C. Composed analytical models for seismic assessment of reinforced concrete bridge columns. *Earthquake Engineering & Structural Dynamics*, 2015, 44(2):265-281.

[8] SHORAKA M B, YANG T Y, ELWOOD K J. Seismic loss estimation of non-ductile reinforced concrete buildings. *Earthquake Engineering & Structural Dynamics*, 2013, 42(2):297-310.

[9] PADGETT J E, DENNEMANN K, GHOSH J. Risk-based seismic life-cycle cost–benefit (LCC-B) analysis for bridge retrofit assessment. *Structural Safety*, 2010, 32(3):165-173.

[10] ZAKERI B, PADGETT J E, AMIRI G G. Fragility analysis of skewed single-frame concrete box-girder bridges. *Journal of Performance of Constructed Facilities*, 2014, 28(3):571-582.

[11] RAMANATHAN K, DESROCHES R, PADGETT J E. A comparison of pre- and post-seismic design considerations in moderate seismic zones through the fragility assessment of multi span bridge classes. *Engineering Structures*, 2012, 45(15):559-573.

[12] MAZZONI S, MCKENNA F, SCOTT M H, et al. OpenSees command language manual. *Pacific Earthquake Engineering Research (PEER) Center*, 2006.

[13] LIEL A B. Assessing the collapse risk of California's existing reinforced concrete frame structures: metrics for seismic safety decisions. *California: Stanford University*, 2008.

[14] BAKER J W. Efficient analytical fragility function fitting using dynamic structural analysis. *Earthquake Spectra*, 2013, 31(1):579-599.

[15] EADS1 L, MIRANDA E, KRAWINKLER H, et al. An efficient method for estimating the collapse risk of structures in seismic regions. *earthquake engineering & structural dynamics*,2013, 42:25–41.

[16] HUANG Chao, LIANG Xingwen. A simplified method for evaluating the seismic risk of FRC frame structures. *Engineering Mechanics*, 2017, 34(7):117-125.

[17] American Society of Civil Engineers (ASCE/SEI 41–06). Seismic rehabilitation of existing buildings. *American Society of Civil Engineers*: Reston, Virginia, 2013.

[18] ELWOOD K J, EBERHARD M O. Effective stiffness of reinforced concrete columns. *ACI Structural Journal*, 2009, 106(4):476–484.

[19] BERRY M P , EBERHARD M O. Practical performance model for bar buckling. *Journal of Structural Engineering*, 2005, 131(7):1060-1070.

[20] ZHU L, ELWOOD K J, HAUKAAS T. Classification and seismic safety evaluation of existing reinforced concrete columns. *Journal of Structural Engineering*, 2007, 133(9): 1316-1330.

[21] WIGHT J K, SOZEN M A. Shear Strength Decay in Reinforced Concrete Columns Subjected to Large Deflection Reversals. *University of Illinois, Urbana-Champaign*, 1975: 1053–1065.

[22] NAGASAKA T. Effectiveness of steel fiber as web reinforcement in reinforced concrete columns, transactions of the japan concrete institute, 1982, 4(1):493-500.

[23] IMAI H, YAMAMOTO Y. A Study on Causes of Earthquake Damage of Izumi High School Due to Miyagi-Ken-Oki Earthquake in 1978. *Transactions of the Japan Concrete Institute*, 1986, pp.405-418.

[24] ARAKAWA T, HE M X, ARAI Y et al, Shear Resisting Behavior of Reinforced Concrete Columns with Spiral Hoops[R]. *Transactions of the Japan Concrete Institute*, 1998, pp. 155-162.

[25] ANG B G, PRIESTLEY M J N, PAULAY T. Seismic shear strength of circular reinforced concrete columns. *ACI structural journal*, 1989, 86(1):45-59.

[26] LYNN A. Seismic Evaluation of Existing Reinforced Concrete Building Columns. *Berkley: University of California*, Berkeley, 1999.

[27] SEZEN H, MOEHLE J P. Shear Strength Model for Lightly Reinforced Concrete Columns. *Journal of Structural Engineering*, 2004.130:1692-1703.

[28] DAVEY B E. Reinforced concrete bridge piers under seismic loading. *Christchurch: University of Canterbury*, 1975.

[29] MUNRO I R M, PARK R, PRIESTLEY M J N. Seismic behavior of reinforced concrete bridge piers, *University of Canterbury, Christchurch, New Zealand*, 1976: 76-89.

[30] ANG B G, PRIESTLEY M J N, PARK R. Ductility of Reinforced Concrete Bridge Piers Under Seismic Loading, *University of Canterbury, Christchurch, New Zealand*, February 1981.

[31] KUNNATH S K, BRACCI J M, ATAHAN A. Analytical Modeling of Beam-Column Joints of Composite SRC Frame Systems. *Earthquake Resistant Structures*, 1998.

[32] JT/T663-2006. Series of elastomeric pad bearings for highway bridges. *Beijing: China Communications Press*, 2006. (in Chinese)

[33] CHEN Libo. Seismic fragility analysis for highway bridges in Wenchuan region. *ChenDu. Southwest Jiaotong University*,2012. (in Chinese)

[34] AVIRAM A, MACKIE K R, STOJADINOVIĆ B. Guidelines for nonlinear analysis of bridge structures in California. *Pacific Earthquake Engineering Research Center*, 2008:25-29.

[35] RAMANATHAN K, PADGETT J E, DESROCHES R. Temporal evolution of seismic fragility curves for concrete box-girder bridges in California. *Engineering Structures*, 2015, 97:29-46.

[36] Ministry of Communications of the People's Republic of China. The criterion for seismic design of highway engineering: trial. *Beijing: China Communications Press*, 1977. (in Chinese)

[37] JTG/T B02-01-2008, Guideline for seismic design for highway bridges. *Beijing: China Communications Press*, 2008. (in Chinese)

[38] LI Yanghai. A practical handbook for highway bridge support. *Beijing: China Communications Press,* 2008. (in Chinese)

[39] MARONEY B H. Large scale bridge abutment tests to determine stiffness and ultimate strength under seismic loading. *University of California, Davis*, 1995.

[40] QIAO Minyuan. Research on bridge seismic responses under the excitation of near-fault ground motions. *Beijing: Beijing Jiaotong university*,2013. (in Chinese)

[41] Federal Emergency Management Agency (FEMA). *Recommended methodology for quantification of building system performance and response parameters, Project ATC-63, Prepared by the Applied Technology Council, Redwood City, CA* 2009.

[42] SHEN Jumin. Seismic Engineering. *Beijing: China Building Industry Press*, 2015.